Comparison of laser-induced breakdown spectra of organic compounds with irradiation at 1.5 and 1.064 μm

Diane M. Wong and Paul J. Dagdigian*

Department of Chemistry, The Johns Hopkins University, Baltimore, Maryland 21218-2685

*Corresponding author: pjdagdigian@jhu.edu

Received 17 June 2008; revised 29 August 2008; accepted 3 September 2008;
posted 4 September 2008 (Doc. ID 97536); published 9 October 2008

A comprehensive investigation of laser-induced breakdown spectroscopy (LIBS) at 1.500 μm of residues of six organic compounds (anthracene, caffeine, glucose, 1,3-dinitrobenzene, 2,4-dinitrophenol, and 2,4-dinitrotoluene) on aluminum substrates is presented and compared with LIBS at the Nd:YAG fundamental wavelength of 1.064 μm. The overall emission intensities were found to be smaller at 1.500 μm than at 1.064 μm, and the ratios of C_2 and CN molecular emissions to the H atomic emissions were observed to be less. Possible reasons for the observed differences in LIBS at 1.064 μm versus 1.500 μm are discussed.

OCIS codes: 140.3440, 300.6360, 300.2140.

1. Introduction

Laser-induced breakdown spectroscopy (LIBS) has emerged as a powerful technique for the detection and characterization of materials such as residues of organic compounds, including explosives, on surfaces [1,2]. The overwhelming majority of modern LIBS experiments employ either the Nd:YAG fundamental beam at 1064 nm or one of its harmonics (532, 355, 266 nm) as the laser source. This laser is particularly convenient for portable sensors because of its small size and power requirements. However, the fundamental wavelength (1064 nm) has a very low threshold for damage to the eye as compared to slightly longer wavelengths of 1.5–1.6 μm [3]. This 1.5–1.6 μm spectral range is also advantageous because it lies within an atmospheric "window," for which there is little absorption by molecules present in air. To our knowledge, there is only one published report on LIBS with laser irradiation in this spectral region, namely, a brief study by Bauer *et al.* [4]. In this work, LIBS with 1.064 μm irradiation was compared with irradiation at longer wavelengths. The authors state, without much detail, that the energy required to generate a laser-induced plasma is lower at the longer wavelengths, from 1.064 to 1.470 μm. They also report a preliminary LIBS spectrum for laser irradiation at 1.470 μm.

In the present study, we compare LIBS spectra of organic residues on aluminum substrates obtained from plasmas generated at two separate irradiation wavelengths, 1.064 and 1.500 μm. Since the laser beams were of the same energy and transverse beam profile, the relative intensities of the atomic emission lines and the overall signal strength for these two wavelengths could be directly compared. A set of organic compounds with differing atomic molar ratios and chemical structure was investigated.

2. Experimental

A schematic drawing of the apparatus for these LIBS experiments is presented in Fig. 1. The pulsed laser radiation for generating the plasma was obtained from the idler output of an optical parametric oscillator (OPO) system (Continuum Panther). This OPO was pumped by 290 mJ of the 355 nm tripled output of an injection-seeded Nd:YAG laser system

0003-6935/08/31G149-09$15.00/0

Report Documentation Page

Form Approved
OMB No. 0704-0188

1. REPORT DATE	2. REPORT TYPE	3. DATES COVERED
2008		**00-00-2008 to 00-00-2008**

4. TITLE AND SUBTITLE	5a. CONTRACT NUMBER
Comparison of laser-induced breakdown spectra of organic compounds with irradiation at 1.5 and 1:064 μm	**W911NF-06-1-0446**
	5b. GRANT NUMBER
	5c. PROGRAM ELEMENT NUMBER
6. AUTHOR(S)	5d. PROJECT NUMBER
	5e. TASK NUMBER
	5f. WORK UNIT NUMBER
7. PERFORMING ORGANIZATION NAME(S) AND ADDRESS(ES) **Department of Chemistry,The Johns Hopkins University,Baltimore,MD,21218-2685**	8. PERFORMING ORGANIZATION REPORT NUMBER **; 50351.14**
9. SPONSORING/MONITORING AGENCY NAME(S) AND ADDRESS(ES) **U.S. Army Research Office, P.O. Box 12211, Research Triangle Park, NC, 27709-2211**	10. SPONSOR/MONITOR'S ACRONYM(S)
	11. SPONSOR/MONITOR'S REPORT NUMBER(S) **50351.14**

12. DISTRIBUTION/AVAILABILITY STATEMENT
Approved for public release; distribution unlimited

13. SUPPLEMENTARY NOTES

14. ABSTRACT

15. SUBJECT TERMS

16. SECURITY CLASSIFICATION OF:			17. LIMITATION OF ABSTRACT	18. NUMBER OF PAGES	19a. NAME OF RESPONSIBLE PERSON
a. REPORT **unclassified**	b. ABSTRACT **unclassified**	c. THIS PAGE **unclassified**	**Same as Report (SAR)**	**10**	

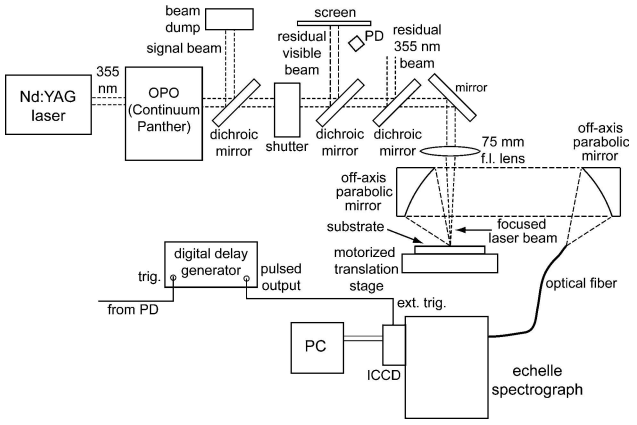

Fig. 1. Schematic diagram of the experimental apparatus. PD denotes photodiode.

(Continuum Precision Powerlite 8000) operated at a 10 Hz repetition rate. The OPO output beam was passed through three dichroic mirrors to remove visible signal beam and residual 355 nm pump beam radiation from the near-IR idler beam. The OPO was tuned by rotating the BBO crystal in the oscillator cavity to yield either 1.500 or 1.064 μm idler radiation.

Single pulses of idler radiation (typically 7 mJ in a 5 mm diameter beam, with a wavelength-independent pulse width of ~6 ns, as measured with a fast photodiode on the signal beam) were passed through a mechanical shutter (Thor Labs) and focused with a fused silica lens (focal length 75 mm) onto an aluminum foil substrate coated with the organic residue under investigation. The foil was mounted on a motorized translation stage, and a fresh area of the residue was irradiated with each laser shot. The position of the lens above the substrate was the same for the two wavelengths. It should be noted that the focal length of the lens, which depends on $n-1$, where n is the refractive index [5], should only differ by 1% between the two wavelengths. The transverse intensity profile of the OPO laser beam had an approximate top-hat shape, and it was not possible to predict *a priori* the focused beam spot size. To get an estimate of the spot sizes at the two wavelengths, areas of laser-induced craters on bare aluminum foil were measured with an optical microscope equipped with a camera. The crater areas were essentially the same at the two wavelengths and were approximately 0.040 mm^2 in magnitude.

The optical emission from the plasma was focused onto a UV-transmitting optical fiber (50 μm core) with a pair of off-axis parabolic mirrors (focal length 25.4 mm). The output of the optical fiber was transmitted to an echelle spectrometer (Andor Mechelle 5000) equipped with a gated, intensified CCD camera (Andor DH 734-18-03). For each compound, the ICCD delay and gate width were optimized for the best signal-to-background ratio, and the same settings were employed for a given compound at both wavelengths. The ICCD delays and gate widths were in the range of 1–3 μs and 5–10 μs, respectively. The ICCD was synchronized with the laser pulse by the output of a digital delay generator (Stanford Research Systems), which was triggered with the output of a photodiode that viewed the residual signal output of the OPO.

The compounds were prepared as residues on aluminum foil substrates. The compounds [anthracene, caffeine, glucose, 1,3-dinitrobenzene (DNB), 2,4-dinitrotoluene (DNT), and 2,4-dinitrophenol (DNP)] were obtained from Sigma-Aldrich, Fluka, or Eastman and were used without further purification. The molecular formulas and atomic molar ratios for the compounds investigated are given in Table 1. For each compound, a 10–50 μl aliquot of a nearly saturated solution in methanol, acetone, or ethanol was delivered to the substrate surface, and the solution was allowed to dry in a chemical fume hood. The resulting spot size was measured to determine the average surface coverage of the compound. The surface concentrations ranged from ~20 to 140 $\mu g/cm^2$ and were approximately the same for a given compound at the two wavelengths.

It is well known that emission on N and O atomic lines in the red appear in laser-induced breakdown spectra in air with ns lasers, because of entrainment of ambient air in the plasma [6,7]. Similarly, CN emission has been observed in LIBS of hydrocarbons in ambient air [8]. Several approaches have been taken to reduce or eliminate signals due to entrainment of air into plasma. Double-pulse LIBS has been shown to reduce significantly the effects of entrainment [6]. As an alternative, observation of prompt emission with irradiation from a low laser fluence has been employed since this signal is relatively uncontaminated by air entrainment [7]. In this study, we have eliminated the contribution to N and O atomic and CN molecular emission due to air entrainment by bathing the substrate with argon gas. This procedure allowed us to record signals on C, H, N, and O lines and the CN bands characteristic of the organic residue only. For bare aluminum substrates, signals due to N and O are not observed. Below we discuss H and C signal levels from the bare substrates. CN and C_2 emission was observed only with organic residues deposited on aluminum foil substrates, and not bare foil.

Table 1. Molecular Formulas and Molar Ratios for the Organic Compounds Investigated

Compound	Formula	Molar Ratio C/H	Molar Ratio O/H	Molar Ratio N/H
Anthracene	$C_{14}H_{10}$	0.714	0	0
Caffeine	$C_8H_{10}N_4O_2$	0.800	0.200	0.400
Glucose	$C_6H_{12}O_6$	0.500	0.500	0
1,3-Dinitrobenzene	$C_6H_4N_2O_4$	1.500	1.000	0.500
2,4-Dinitrophenol	$C_6H_4N_2O_5$	1.500	1.250	0.500
2,4-Dinitrotoluene	$C_7H_6N_2O_4$	1.167	0.667	0.333

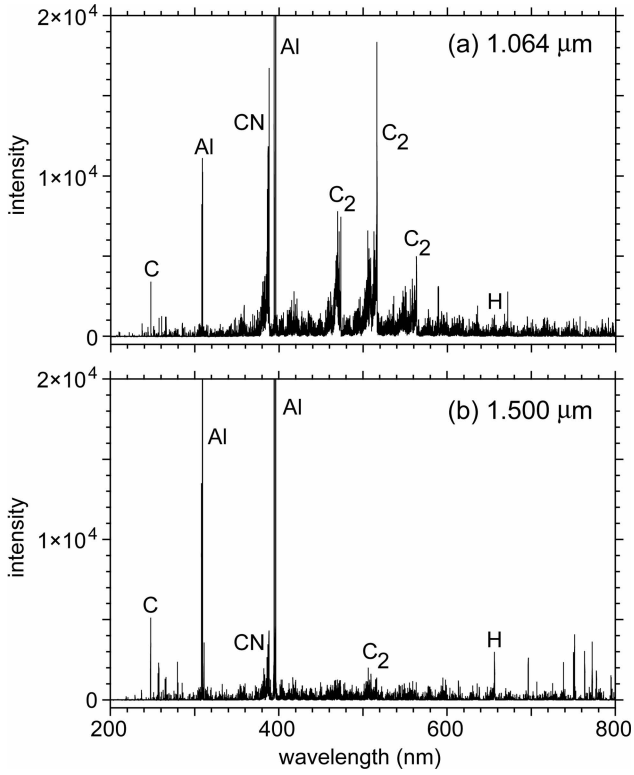

Fig. 2. Survey single-shot LIBS spectra of 2,4-DNT residues (average surface concentration $\sim 75\,\mu g/cm^2$) on aluminum foil for irradiation at (a) 1.064 and (b) 1.500 μm. Prominent emission features are marked: Al, 308 and 394 nm; C, 248 nm; H, 656 nm; CN $B-X\Delta v=0$ sequence, 388 nm; C_2, $d-a$ $\Delta v=+1$, 0, −1 sequences at 474, 516, and 564 nm, respectively. The lines in the 700–800 nm spectral range are mainly due to the argon bath gas.

3. Results

In Fig. 2, we present examples of single-shot LIBS spectra of 2.4-DNT irradiated at 1.064 and at 1.500 μm. Both spectra were taken under the same experimental conditions, except for the irradiation wavelength. The strongest lines in the spectra are at 394 and 308 nm and can be identified as atomic Al transitions originating from the aluminum foil substrate. Lines from the argon bath gas can be seen in the 700–800 nm spectral range. The C and H atomic emission lines from the DNT residue, seen near 248 and 656 nm, respectively, are clearly visible in the spectra. N and O atomic lines in the red are present in the spectra but are obscured by the stronger Ar lines. Several molecular emission features are observable in the spectra, including the CN $B-X$ $\Delta v=0$ sequence near 388 nm and the $\Delta v=+1$, 0, and −1 sequences of the C_2 $d-a$ band system (Swan bands) near 516 nm. The off-diagonal CN $B-X$ $\Delta v=+1$ and −1 sequences have small Franck–Condon factors and are hence barely visible in the spectra.

It can be seen that the CN and C_2 bands are particularly strong in the DNT spectrum for irradiation at 1.064 μm, displayed in Fig. 2(a). By contrast, these bands are much weaker for irradiation at 1.500 μm [see Fig. 2(b)]. The differences in the intensities of features in the two spectra displayed in Fig. 2 suggest that there are significant differences in LIBS spectra with irradiation at 1.500 versus 1.064 μm.

For a quantitative comparison of LIBS spectra at the two wavelengths, two sets of 25 single-shot spectra were recorded for each compound at each wavelength. For each spectrum, the intensities of the transitions listed in Table 2 were measured. While several sequences of the C_2 $d-a$ band system were visible in the spectrum displayed in Fig. 2(a), we measured the intensity of only the strongest, namely, the $\Delta v=0$ sequence, since the C_2 emission was weak or not detectable in some spectra. For the stronger features, both peak areas and heights were measured, and their ratios were found to be consistent to within ~2%. For weaker features, notably the N atomic lines, areas could not be reliably determined. We hence employed peak heights as the measure of intensity for all transitions. For CN and C_2, the heights of the (0,0) band heads were measured. Since the N atomic lines were weak, the intensities of the three lines (see Table 2) were summed in order to have a more reliable estimate of the N atomic intensity. In all cases, intensities were corrected for background continuum emission. No correction for the wavelength-dependent response of the detection system was carried out.

We inspected bare aluminum foil substrates for spectral features due to unintentional organic contamination. The foil substrates were carefully handled with forceps to minimize the contact with fingers and to prevent the transfer of oils from the fingertips onto the surface of the clean aluminum foil. In some cases, weak emission on C and H atomic lines was observed; however, these signals were negligible compared to the intensities with an organic residue on the substrate. We did observe varying intensities of both the C and H lines due to organic residues with different commercial sources of aluminum substrate, in particular with an aluminum sheet of quoted purity 99.998% (metals basis) bought from Alfa Aesar.

It is well known that LIBS intensities vary significantly from shot to shot, as was the case in the present experiment. It has been found that measurement of ratios of intensities yields more robust results [9–13]. We hence determined ratios of intensities in each single-shot spectrum. These ratios were then averaged for each set of 25 single-shot spectra.

Table 2. Spectral Transitions Used for Quantitative Analysis of LIBS Spectra of Organic Compounds

Species	Wavelength (nm)	Transition
H	656.3	$n=3\rightarrow n=2$
C	247.9	$2p3s\,^1P_1\rightarrow 2p^2\,^1D_2$
O	777.2–5	$3p\,^5P_{1,2,3}\rightarrow 3s\,^5S_2$
N	742.4	$3p\,^4S_{3/2}\rightarrow 3s\,^4P_{1/2}$
N	744.2	$3p\,^4S_{3/2}\rightarrow 3s\,^4P_{3/2}$
N	746.8	$3p\,^4S_{3/2}\rightarrow 3s\,^4P_{5/2}$
C_2	516.3	$d-a$ $\Delta v=0$
CN	388.3	$B-X$ $\Delta v=0$

No spectra were discarded in computing average intensity ratios. Since the H line was usually the strongest atomic feature originating from the organic residues, ratios of intensities with respect to the H atomic line were computed.

Figure 3 presents the measured ratios of the C, O, and N atomic line intensities (peak heights) to the H atomic line intensity for both data sets of each of the organic compounds investigated at the two irradiation wavelengths. Similarly, Fig. 4 presents the measured ratios of molecular emission intensities, involving C_2 and CN, to the H atomic line intensity. We see from Figs. 3 and 4 that, with a few exceptions, there is good consistency between the ratios

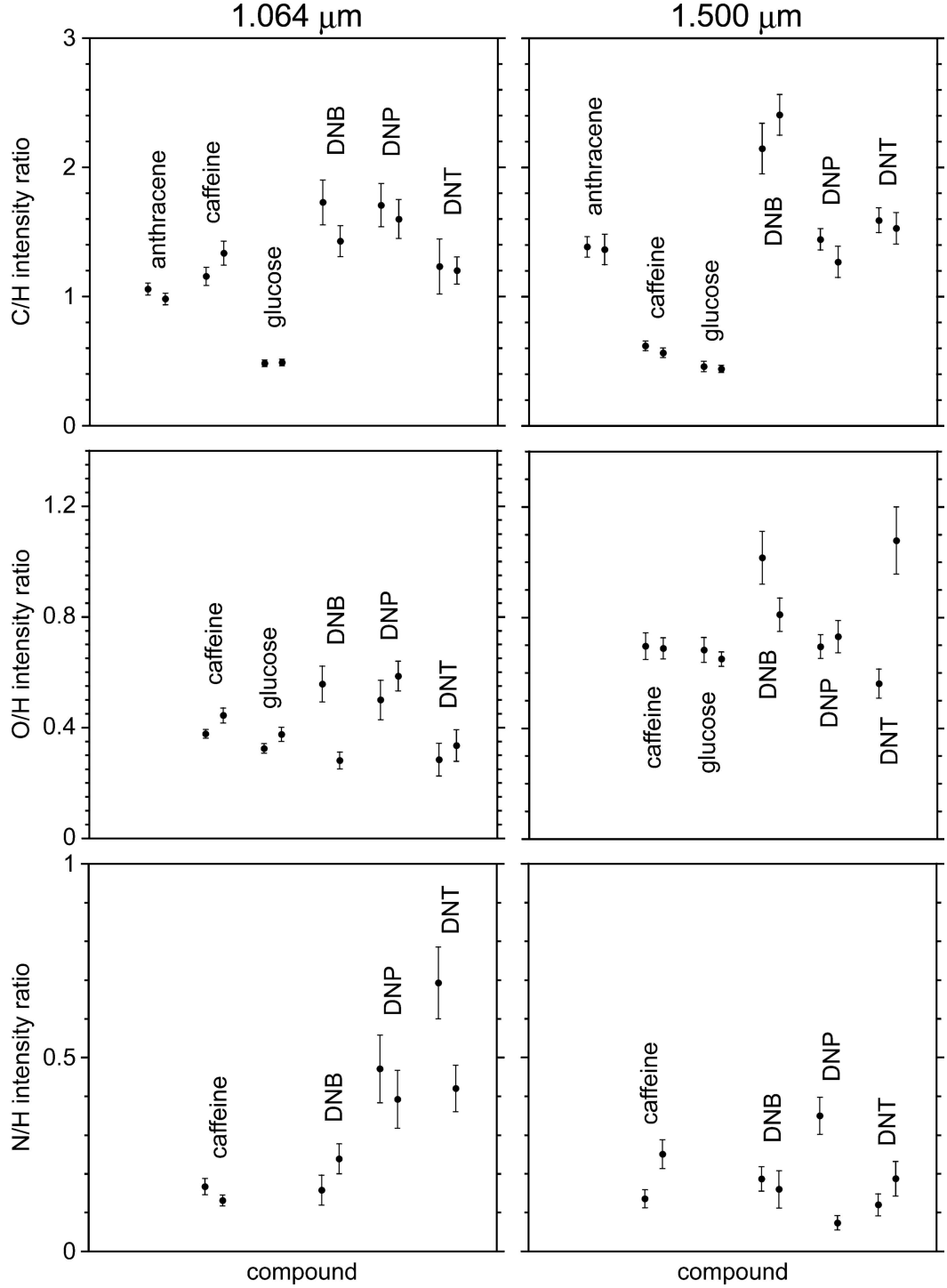

Fig. 3. Ratios of C, O, and N line intensities (peak heights) to the H atomic line intensity for LIBS of organic residues on aluminum foil substrates. The spectra were recorded under identical conditions except for the irradiation wavelengths, which are indicated at the top of the sets of panels. The two plotted points for each compound represent means of the intensity ratios for two sets of 25 single-shot spectra; the error bars are the standard deviations of the mean.

determined for the two data sets of each compound and wavelength.

The dinitro compounds displayed the largest C/H intensity ratios for both irradiation wavelengths, but the ratios were not dramatically greater than those of the other compounds. There were only slight differences in the C/H intensity ratios for a given compound between the two wavelengths. The O/H intensity ratios at a given wavelength were similar for the compounds investigated. For all the compounds, the O/H intensity ratios were larger for irradiation at 1.500 μm than at 1.064 μm, but again the differences between the two wavelengths were not great. At 1.064 μm, DNP and DNT displayed the largest N/H intensity ratios; these ratios were significantly smaller at 1.500 μm. Caffeine and DNB had similar, small N/H intensity ratios at both wavelengths.

We observe that the measured C/H intensities at both irradiation wavelengths roughly correlate with the molar C/H ratios of the compounds investigated (compare Fig. 3 with Table 1). However, such a correlation does not apply to the O/H and N/H ratios.

The most dramatic differences in intensity ratios between the two wavelengths are seen in the ratios of the molecular (CN and C_2) features to H atomic intensity (see Fig. 4). We observe C_2 emission only for the aromatic organic compounds. Strong C_2 emission has previously been reported for LIBS of this class of compounds and been found to increase with increasing numbers of fused aromatic rings [8,14]. DNT has by far the largest C_2/H intensity ratio (~16) for irradiation at 1.064 μm. In marked contrast, the C_2/H intensity ratios for all the aromatic compounds at 1.500 μm are much smaller, approaching unity. In fact, DNT has the smallest C_2/H intensity ratio at this wavelength.

Similar, large differences are observed for the ratios of CN to H emission for irradiation at 1.064 versus 1.500 μm. For LIBS at 1.064 μm, the

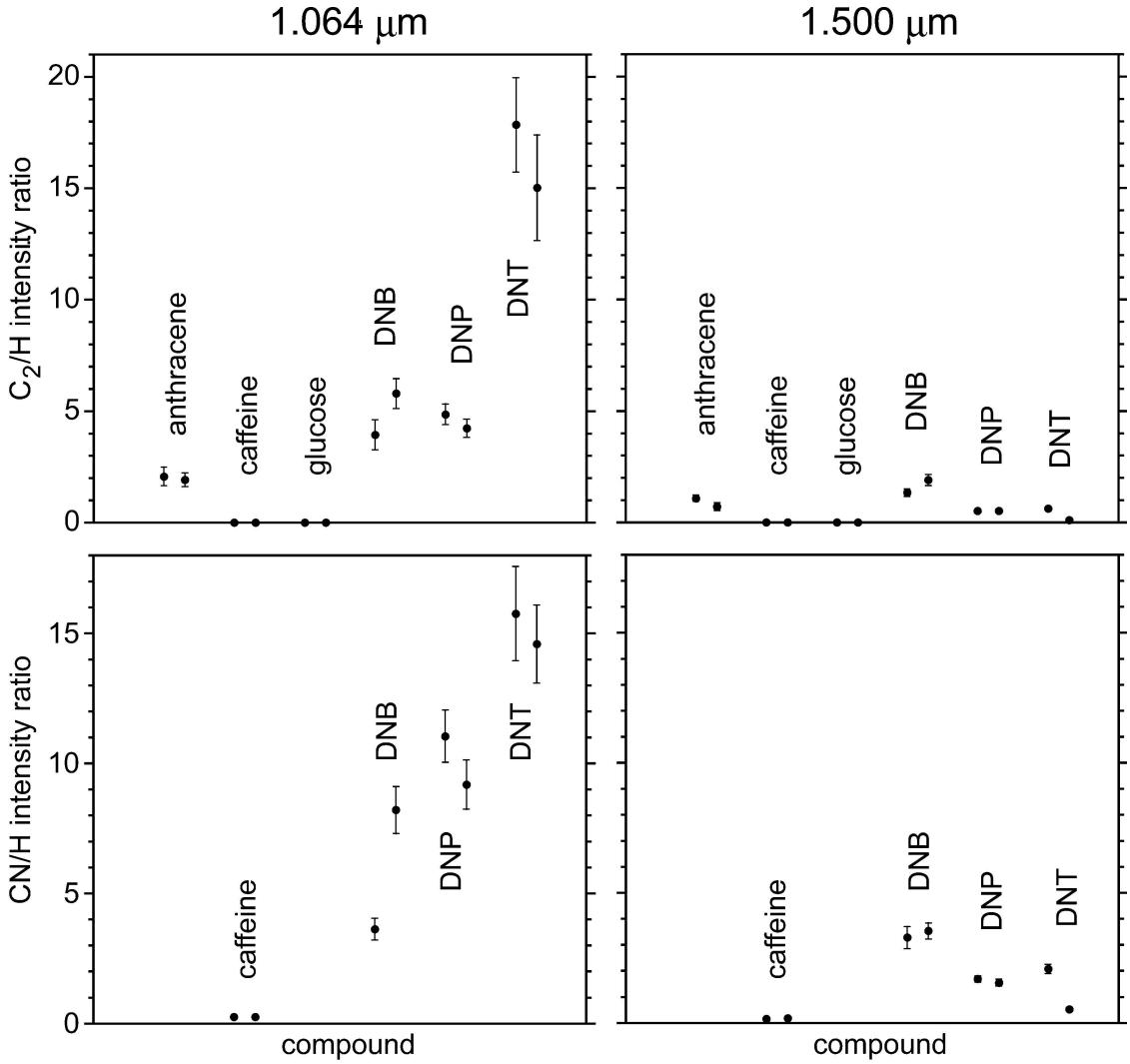

Fig. 4. Ratios of C_2 and CN (0,0) band head intensities to the H atomic line intensity for LIBS of organic residues on aluminum foil substrates. The spectra were recorded under identical conditions except for the irradiation wavelengths, which are indicated at the top of the sets of panels. The two plotted points for each compound represent means of the intensity ratios for two sets of 25 single-shot spectra; the error bars are the standard deviations of the mean.

nitrogen-containing aromatic compounds display CN/H intensity ratios ranging from ~6 to 15. The corresponding intensity ratios are seen in Fig. 4 to be much smaller at 1.500 μm. The only other nitrogen-containing molecule, caffeine, showed small CN/H ratios at both wavelengths.

It is also of interest to compare the overall intensities at the two irradiation wavelengths. Of the atomic lines, the H atomic line is the most appropriate to consider since the intensity ratios displayed in Figs. 3 and 4 are referenced to this line. Figure 5 displays the absolute H line intensities for both data sets of each of the organic compounds investigated at the two irradiation wavelengths. Since the C_2 and CN emissions are quite strong for the aromatic compounds, the intensities of the bands due to the species are also displayed in the lower panels of Fig. 5.

We see from Fig. 5 that the H atomic line intensity is the strongest for anthracene, caffeine, and glucose at both wavelengths, while the intensity of this line is less for the nitroaromatic compounds. We also observe in Fig. 5 that the H line intensity is approximately a factor of 2 smaller at 1.500 μm than at 1.064 μm for anthracene, caffeine, and glucose, while the H line intensities for the nitroaromatic compounds are only slightly different at the two wavelengths.

Significant differences are found for the absolute intensities of the molecular emissions between the two wavelengths. For all the aromatic compounds, the C_2 and CN emission is significantly smaller at 1.500 μm than at 1.064 μm. At both wavelengths, the C_2 emission is stronger for anthracene than for the nitroaromatic compounds. We also observe that the CN emission is weaker at both wavelengths for caffeine than the nitroaromatic compounds.

Some comments about the intensity of Al atomic transitions, which arise from ablation of the aluminum foil substrate, are in order. We do observe some variation in the intensities of the 394 and 308 nm Al atomic transitions for the different organic residues at a given irradiation wavelength. However, there were no dramatic differences in the intensities of these transitions between the two wavelengths.

For the interpretation of these results, it is useful to estimate the temperature and electron density of the plasmas generated at the two irradiation wavelengths. We have utilized the ratio of the intensities of the Al atomic lines at 394.4 and 308.2 nm for the determination of temperature, similar to the determinations carried out by Piehler *et al.* [15] in a study of LIBS of aluminum in various bath gases. The ratio of the intensities I of the two lines can be employed to estimate the plasma temperature with the following equation:

$$\frac{I_1}{I_2} = \frac{g_1 A_1 \lambda_2}{g_2 A_2 \lambda_1} \exp\left(-\frac{E_1 - E_2}{kT}\right), \qquad (1)$$

Here, g_i and E_i are the statistical weight and energy, respectively, of the upper level of line i and λ_i is the wavelength of the line. The radiative transition probabilities A_i were taken from the NIST Atomic Spectra Database [16].

Temperatures were determined in this way for LIBS of residues of two of the organic compounds, namely, anthracene and DNT. These are presented in Table 3. The reported temperatures, which were obtained from intensities measured with fairly wide detector gates (see Table 3), are similar to those reported by Piehler *et al.* [15] for delay times of ~10 μs. In this experiment, somewhat higher laser powers were employed (35 mJ of 1.064 μm radiation focused with a 50 mm focal length lens). Of most interest for the interpretation of our measured LIBS intensities is the comparison of the temperatures for the two irradiation wavelengths. We see from Table 3 that for both compounds the temperature deduced for irradiation at 1.500 μm is noticeably higher than for irradiation at 1.064 μm.

An estimate of the electron density can be obtained from the observed broadening of the H atomic line at 656.3 nm. The relationship between electron density and linewidth is well established for many elements [17], and we have employed the tables prepared by Vidal *et al.* [18]. Figure 6 compares the profile of the H atomic 656.3 nm line for irradiation of anthracene and DNT residues at the two wavelengths. It can be seen that for both compounds the profiles for irradiation at 1.500 μm are slightly broader than for 1.064 μm. This was also true for this line with the other compounds investigated. From comparison of the line profiles displayed in Fig. 6 and the profiles computed by Vidal *et al.* [18], we estimate that the electron density, averaged over the detection gate (see Table 3), was 6×10^{16} and 8×10^{16} cm^{-3} for irradiation of anthracene at 1.064 and 1.500 μm, respectively. The corresponding electron densities for DNT were 3×10^{16} and 4×10^{16} cm^{-3}. We hence find slightly higher electron densities for irradiation at 1.500 μm than at 1.064 μm.

4. Discussion

This study is to our knowledge the first comprehensive study of LIBS at 1.5 μm. It is perhaps not unexpected that we were able to obtain LIBS spectra at this irradiation wavelength since laser radiation of sufficiently high intensity at any wavelength should cause ablation, and also formation of plasma, at a surface. Of greater importance is the quantitative comparison between LIBS at 1.500 μm and at the Nd:YAG fundamental wavelength of 1.064 μm. From the absolute intensities displayed in Fig. 5 and the intensity ratios displayed in Figs. 3 and 4, we see that the overall LIBS intensity is significantly smaller at 1.500 μm than at 1.064 μm for the investigated organic residues on aluminum substrates. We also find significantly different ratios of intensities of various emission features in LIBS spectra at the two wavelengths. The most dramatic differences are in the ratios of the intensities of the C_2 and CN molecular bands relative to the H atomic line intensity for

the aromatic compounds. Moreover, the absolute intensities of these bands are smaller at 1.500 μm than at 1.064 μm.

The weaker emission intensities for irradiation at 1.500 μm as compared to those for irradiation at 1.064 μm could be due to differences in a variety of parameters, including the amount of material ablated, plasma temperature, and electron density of the laser-induced plasma. Amoruso *et al.* [19] have presented a comprehensive review of laser-ablation

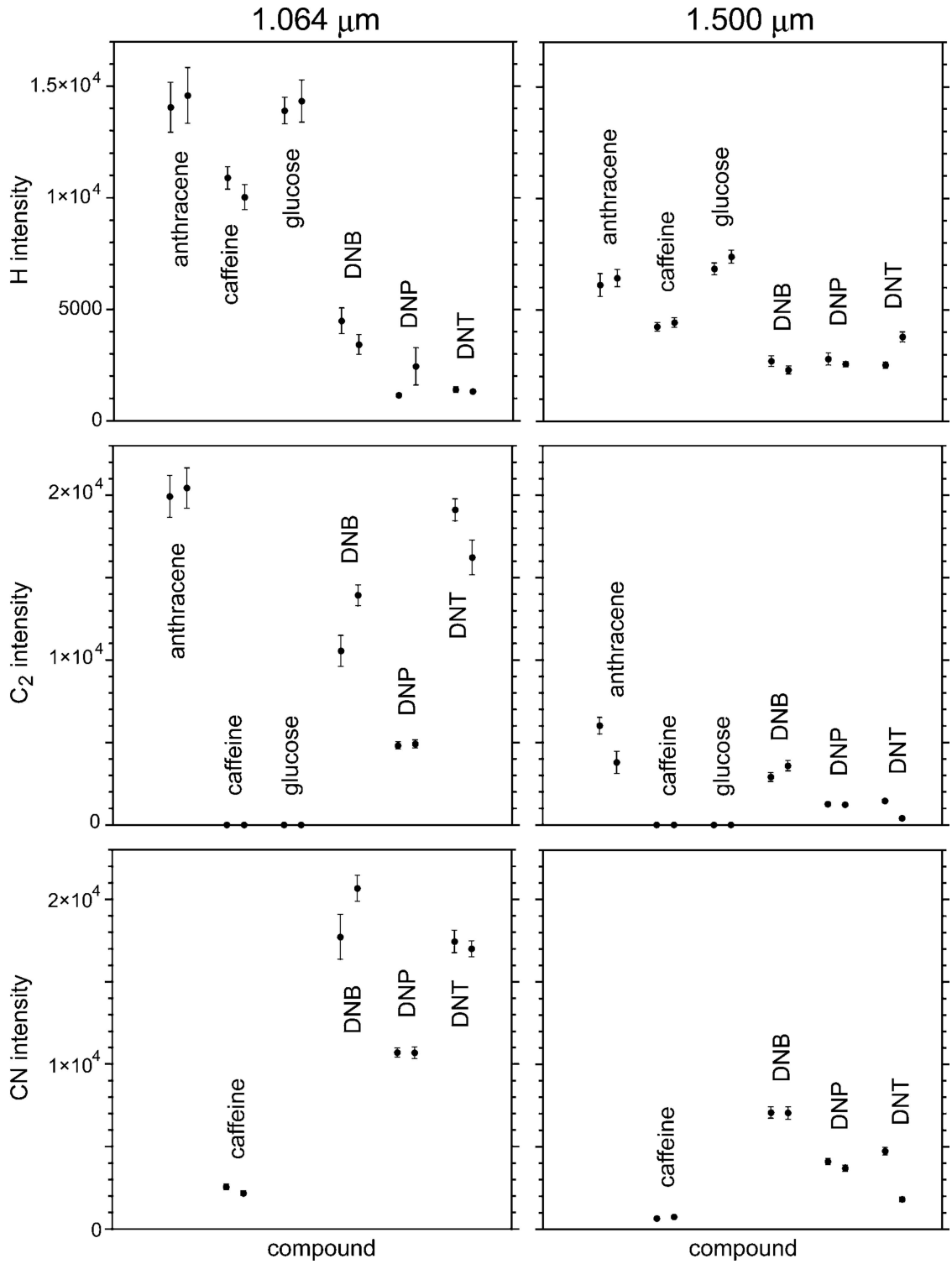

Fig. 5. Intensities of the H atomic line and the C_2 and CN (0,0) band heads for LIBS of organic residues on aluminum foil substrates. The spectra were recorded under identical conditions except for the irradiation wavelengths, which are indicated at the top of the sets of panels. The two plotted points for each compound represent means of the intensity ratios for two sets of 25 single-shot spectra; the error bars are the standard deviations of the mean.

plasmas and have discussed ablation and formation of a plasma by irradiation with pulsed laser radiation of ns duration. The leading edge of the laser pulse is absorbed by the substrate, and there is sufficient time for thermal diffusion into a zone larger than the focused laser spot size. The organic residues prepared in this study were thin enough that the laser energy is absorbed predominantly by the conduction electrons in the underlying aluminum substrate. This energy is transferred to the lattice, and neutral and ionized species evaporate from the surface. The ns laser pulse is sufficiently long that the incipient plasma absorbs radiation from the tail of the laser pulse by the inverse bremsstrahlung process [20], heating the plasma and shielding the substrate from further ablation.

The absorption of laser energy by the aluminum substrate should not differ greatly between the two laser wavelengths (1.064 versus 1.500 μm) employed in this study. However, inverse bremsstrahlung absorption by the plasma will be greater at the longer wavelength [20]. This additional energy uptake by the plasma perhaps provides an explanation for our higher observed temperatures and electron densities at 1.500 μm (see Table 3 and Fig. 6). This would appear to be inconsistent with the fact that emission intensities were found to be lower at 1.500 μm than at 1.064 μm, since an increased temperature and electron density would be expected to lead to higher emission intensities, all other parameters remaining unchanged. It may be that less material is ablated from the sample at 1.500 μm because of the increased shielding by the plasma at this wavelength.

The final observation to be discussed is the significantly reduced molecular emission for irradiation at 1.500 μm as compared to emission at 1.064 μm. The molecular species C_2 and CN can arise from fragmentation of the parent compound or recombination of the atoms in the plasma [7,14,21]. Baudelet *et al.* [7] have noted that it should be possible to distinguish emission from these two mechanisms by varying the detector gate delay. With the relatively long delays employed in the present study, the observed molecular emission is probably due to atomic recombination. The reduced molecular emission at 1.500 μm could be the result of lower atomic concentrations from the increased plasma shielding discussed above, since the molecular concentration will depend nonlinearly on the atomic concentrations. It would be interesting to follow the time dependence of the molecular emissions with a narrower detector gate, but this is beyond the scope of this investigation.

Table 3. Temperatures Determined from Relative Intensities of the Al Atomic 394.40 and 308.22 nm Lines for LIBS Plasmas

	Irradiation Wavelength	
Compound	1.064 μm	1.500 μm
Anthracene[a]	3580 ± 80	3980 ± 80
2,4-Dinitrotoluene[b]	3160 ± 50	3940 ± 60

[a]Detector gate delay and width 1.25 and 7 μs, respectively.
[b]Detector gate delay and width 1.25 and 10 μs, respectively.

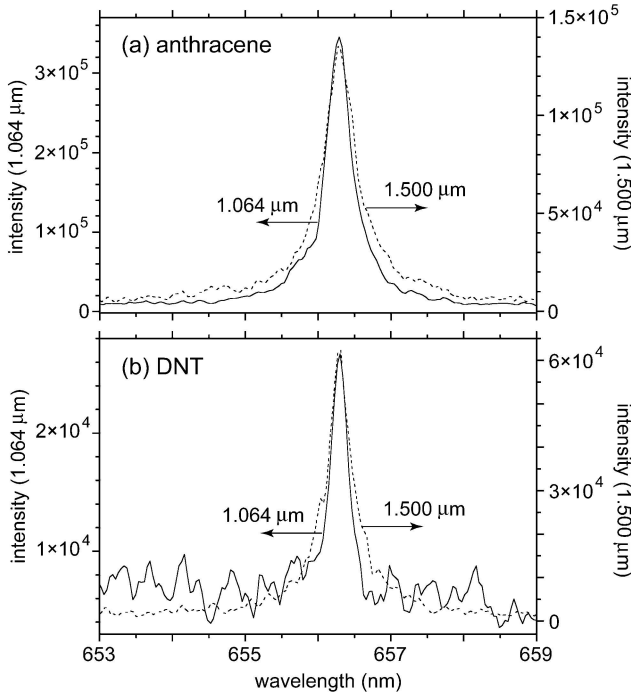

Fig. 6. Profiles of the H atomic line at 656.3 nm, averaged over 25 single-shot spectra, for LIBS at 1.064 μm (solid lines) and 1.500 μm (dotted lines) of anthracene and DNT residues on aluminum foil substrates.

5. Conclusion

A comprehensive investigation of LIBS at 1.500 μm of organic residues on aluminum substrates has been presented and compared with LIBS at the Nd:YAG fundamental wavelength 1.064 μm. The overall emission intensities were found to be smaller at 1.500 μm than at 1.064 μm, and the ratios of molecular to atomic emissions were observed to be less. This result could have implications for the detection sensitivity of LIBS at 1.500 μm. It would be desirable to carry out a similar comparison of LIBS at these wavelengths with higher-power laser radiation. This will require a different laser system as the maximum pulse energy at 1.500 μm of the OPO employed in this study is ~7 mJ.

The authors greatly acknowledge the advice given to us by the LIBS group at the Army Research Laboratory (A. W. Miziolek, K. L. McNesby, F. C. DeLucia, Jr., J. L. Gottfried, and C. A. Munson) at Aberdeen Proving Ground, Maryland, on the acquisition of LIBS spectra. The loan of a motorized translation stage by J. B. Spicer is also gratefully appreciated. This research has been supported in part by the U.S. Army Research Office under grant W911NF-06-1-0206.

References

1. A. W. Miziolek, V. Palleschi, and I. Schechter, eds., *Laser-Induced Breakdown Spectroscopy (LIBS): Fundamentals and Applications* (Cambridge U. Press, 2006).
2. D. A. Cremers and L. J. Radziemski, *Handbook of Laser-Induced Breakdown Spectroscopy* (Wiley, 2006).
3. American National Standards Institute, *American Standard for Safe Use of Lasers* (Laser Institute of America, 2000).
4. C. Bauer, P. Geiser, J. Burgmeier, G. Holl, and W. Schade, "Pulse laser surface fragmentation and mid-infrared laser spectroscopy for remote detection of explosives," Appl. Phys. B **85**, 251–256 (2006).
5. D. E. Gray, ed., *American Institute of Physics Handbook* (McGraw-Hill, 1972).
6. F. C. DeLucia, Jr., J. L. Gottfried, C. A. Munson, and A. W. Miziolek, "Double-pulse laser-induced breakdown spectroscopy of explosives: Initial study towards improved discrimination," Spectrochim. Acta Part B **62**, 1399–1404 (2007).
7. M. Baudelet, M. Boueri, J. Yu, S. S. Mao, V. Piscitelli, X. Mao, and R. E. Russo, "Time-resolved ultraviolet laser-induced breakdown spectroscopy for organic material analysis," Spectrochim. Acta Part B **62**, 1329–1334 (2007).
8. A. Portnov, S. Rosenwaks, and I. Bar, "Emission following laser-induced breakdown spectroscopy of organic compounds in ambient air," Appl. Opt. **42**, 2835–2842 (2003).
9. R. Sattmann, I. Mönch, H. Krause, R. Noll, S. Couris, A. Hatziapostolou, A. Mavrromanolakis, C. Fotakis, E. Larrauri, and R. Miguel, "Laser-indeuced breakdown spectroscopy for polymer identification," Appl. Spectrosc. **52**, 456–461 (1998).
10. M. Tran, Q. Sun, B. W. Smith, and J. D. Winefordner, "Determination of C:H:O:N ratios in solid organic compounds in laser-induced plasma spectroscopy," J. Anal. At. Spectrom. **16**, 628–632 (2001).
11. L. St.-Onge, E. Kwong, M. Sabsabi, and E. B. Vadas, "Quantitative analysis of pharmaceutical products by laser-induced breakdown spectroscopy," Spectrochim. Acta Part B **57**, 1131–1140 (2002).
12. F. Ferioli, P. V. Puzinauskas, and S. G. Buckley, "Laser-induced breakdown spectroscopy for on-line engine equivalence ratio measurements," Appl. Spectrosc. **57**, 1183–1189 (2003).
13. S. Kaski, H. Häkkänen, and J. Korppi-Tommola, "Determination of Cl/C and Br/C ratios in pure organic solids using laser-induced plasma spectroscopy in near vacuum ultraviolet," J. Anal. At. Spectrom. **19**, 474–478 (2004).
14. L. St.-Onge, R. Sing, S. Béchard, and M. Sabsabi, "Carbon emission following 1.064 μm laser ablation of graphite and organic samples in ambient air," Appl. Phys. A **69**, S913–S916 (1999).
15. T. N. Piehler, F. C. DeLucia Jr., C. A. Munson, B. E. Homan, A. W. Miziolek, and K. L. McNesby, "Temporal evolution of the laser-induced breakdown spectroscopy spectrum of aluminum metal in different bath gases," Appl. Opt. **44**, 3654–3660 (2005).
16. NIST Atomic Spectra Database, version 3 NIST Atomic Spectra Database, version 3. http://physics.nist.gov/PhysRefData/ASD.
17. H. R. Griem, *Spectral Line Broadening by Plasmas* (Academic, 1974).
18. C. R. Vidal, J. Cooper, and E. W. Smith, "Hydrogen Stark-broadening tables," Astrophys. J. Suppl. Ser. **25**, 37–136 (1973).
19. S. Amoruso, R. Bruzzese, N. Spinelli, and R. Velotta, "Characterization of laser-ablation plasmas," J. Phys. B **32**, R131–R172 (1999).
20. J. F. Ready, *Effects of High Power Laser Radiation* (Academic, 1971).
21. V. I. Babushok, F. C. DeLucia, Jr., P. J. Dagdigian, J. L. Gottfried, C. A. Munson, M. J. Nusca, and A. W. Miziolek, "Kinetic modeling study of the laser-induced plasma plume of the explosive cyclomethylenenitramine (RDX)," Spectrochim. Acta Part B **62**, 1321–1328 (2007).